Article

AILDE Computer-Aided Discovery of Novel Ibuprofen−Coumarin Antitumor Lead Compounds Targeting Cyclooxygenase-2

Fengxu Wu,[⊥] Tianshuai Wang,[⊥] Xiaoyu Tang,[⊥] Sirui Dong, Lun Luo, Chao Luo, Junkai Ma,* and Yanggen Hu*

Read Online

ACCESS | Metrics & More | Article Recommendations | Supporting Information

ABSTRACT: Starting from three ibuprofen−coumarin hit compounds, we designed 18 derivative compounds targeting cyclooxygenase-2 (COX-2) by introducing different substituents onto them by using the computational auto in silico ligand directing evolution (AILDE) method. After synthesizing and testing the activity, we found that 6 representative compounds have micromolar enzyme inhibitory activity against COX-2. Additionally, 16 compounds have shown certain inhibitory activity in cervical cancer cells. Among these compounds, **6c** (IC$_{50}$ = 0.606 μM, HeLa) and **7g** (IC$_{50}$ = 0.783 μM, HeLa) have exhibited excellent activity, which is approximately 10 times better than the commercial drug gefitinib. According to molecular simulation results, the halogen atoms of **6c** and **7g** on the coumarin ring can form halogen bonds with COX-2, which significantly improves their activity compared to their hit compounds **6a** and **7a**. However, the key interactions were lost in binding with COX-1. The calculation results revealed that the two compounds are selective COX-2 inhibitors, with potential selectivity indexes of 6-fold and 5-fold, respectively. The cell-based activity of compounds **6c** and **7g** toward HEK293 cells demonstrates that our compounds possess an acceptable safety toward normal cells. The results indicate that **6c** and **7g** can serve as potential lead compounds for further lucubrate.
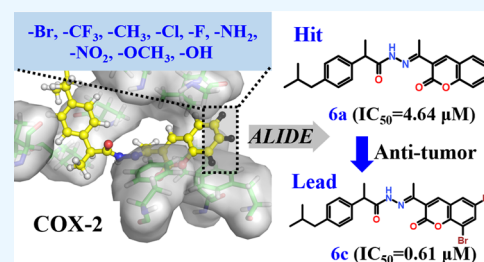
1. INTRODUCTION

Malignant tumors are one of the main reasons for human death around the world. According to statistics, 19.3 million patients were diagnosed in 2020, and the number of deaths reached 9.9 million.[1] At present, chemotherapy is one of the main methods for the treatment of malignant tumors. However, many chemotherapeutics have problems such as multiple drug resistance, high toxicity, and low specificity.[2−4] Therefore, it is imperative to develop novel antitumor drugs with diverse structures, high efficiency, and low toxicity.

Inflammatory response plays an important role in the occurrence and development of tumors, and cyclooxygenase (COX) is one of the important targets that affect inflammatory response.[5−7] COX acts by catalyzing the formation of prostaglandins and related compounds from arachidonic acid with three isomers: COX-1, COX-2, and COX-3.[8,9] Among them, COX-2 is basically not expressed in the normal physiological environment of the body, and its expression level only increases when the body is stimulated.[10] In recent years, many studies have shown that COX-2 is highly expressed in various types of tumor cells, including liver cancer cells, cervical cancer cells, and skin cancer cells.[11−13] It plays a multifaceted role in the occurrence and development of tumors, as well as in the tolerance of tumor cells to chemotherapy and radiation therapy.[14−17]

Ibuprofen is a common COX inhibitor that can be used to treat various diseases in clinical practice.[18,19] It is widely used due to its excellent activity and high safety.[20−22] Due to the high expression of COX-2 in tumor cells and the inhibitory effect of ibuprofen on COX-2, ibuprofen may also have certain antitumor potential. In recent years, researchers have modified the molecular structure of ibuprofen, resulting in compounds exhibiting certain antitumor activity. Shokri et al.[23] coupled ibuprofen with a known targeted peptide sequence NGR, where the NGR peptide can selectively bind to the overexpressed aminopeptidase N in tumor blood vessels and exert its effect. The results of antitumor experiments showed that the NGR-coupled form of ibuprofen had a good inhibitory effect on SKOV-3 tumor cells. Ozlem et al.[24] synthesized a series of derivatives by covalent bonding between lipoic acid and ibuprofen, and the cytotoxicity of newly synthesized derivatives on human glioblastoma cells U87-MG was evaluated. The results showed that the derivatives could effectively inhibit U87-MG, and they had an IC$_{50}$ value of 5.97 μM for U87-MG cell lines.

Natural products are the most important source of new drug development due to their chemical diversity, biological
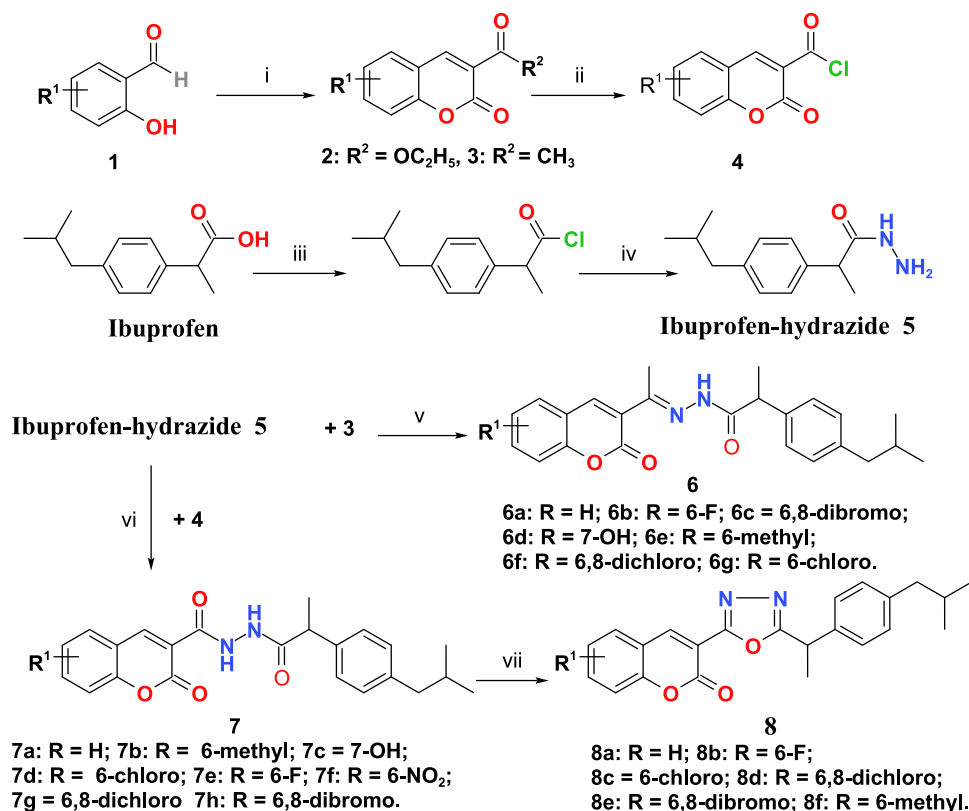
Scheme 1. Synthetic Routes of Compounds 2, 3, 4, 5, 6a−6g, 7a−7h, and 8a−8f[a]

1

2: R[2] = OC$_2$H$_5$, 3: R[2] = CH$_3$

4

Ibuprofen

Ibuprofen-hydrazide 5

Ibuprofen-hydrazide 5 + 3 →v→ 6

6a: R = H; 6b: R = 6-F; 6c = 6,8-dibromo;
6d: R = 7-OH; 6e: R = 6-methyl;
6f: R = 6,8-dichloro; 6g: R = 6-chloro.

vi | + 4

7

7a: R = H; 7b: R = 6-methyl; 7c = 7-OH;
7d = 6-chloro; 7e: R = 6-F; 7f: R = 6-NO$_2$;
7g = 6,8-dichloro 7h: R = 6,8-dibromo.

vii → 8

8a: R = H; 8b: R = 6-F;
8c = 6-chloro; 8d: R = 6,8-dichloro;
8e: R = 6,8-dibromo; 8f: R = 6-methyl.

[a]Reagents and conditions: (i) Diethyl malonate or ethyl acetoacetate, ethanol, reflux; (ii) (1) 1 mol/L NaOH, reflux; (2) 1 mol/L HCl, acidification; (3) SOCl$_2$, rt; (iii) (1) SOCl$_2$, rt; (iv) (1) methanol, rt; (2) hydrazine hydrate, ethanol, reflux; (v) acetic acid-sodium acetate, reflux; (vi) triethylamine, methylene dichloride, 0−5 °C; (vii) phosphorus oxychloride, reflux.

diversity, and druglike properties. Coumarin compounds are an important class of pyranone oxygen-containing heterocyclic compounds with high bioavailability and low toxicity that can be used as lead structural frameworks. Coumarin compounds are widely distributed in plants such as Rutaceae, Umbelliferae, Oleaceae, Meliaceae, Asteraceae, and Orchidaceae. Based on their excellent pharmacological activity, some coumarin derivatives have been approved for clinical treatment.[25−27] Coumarin compounds can exhibit excellent antitumor activity by inhibiting the expression of MMP2 and VEGFA,[28] as well as inhibiting the activities of carbonic anhydrase IX and XII,[29] making them an important research object in antitumor studies.[30−33]

Coumarin has a wide range of applications, and many studies have modified the structure of coumarin to obtain drugs with stronger antitumor activity. Compared with coumarins, hybrid molecules have the potential to reduce cross-resistance, reduce side effects, and improve efficacy and specificity.[34] Pilli et al.[35] synthesized a series of coumarin hydrazone derivatives and screened their anticancer activity against A549, HeLa, SK-NSH, MCF-7 human cancer cells, and normal rat kidney cell NRK-49F using the MTT assay. The results showed that all compounds exhibited good to moderate cytotoxicity, with compounds **12a** and **18a** having the strongest activity. Achar et al.[36] synthesized a series of silver(I) complexes with benzimidazole-based N-heterocyclic carbene ligands, and the drug activity test showed that the compounds had a significant inhibitory effect on human lung cancer cell lines A549 and H1975. Channar et al.[37] designed, synthesized,

and characterized a series of novel benzocoumarin thiazole imine ternary derivatives. The antitumor experimental results showed that the synthesized derivatives had a certain inhibitory effect on cervical cancer HeLa cells, with inhibition rates ranging from 21.0 to 69.7%.

In this study, we used the cyclooxygenase inhibitor ibuprofen as the precursor and designed and synthesized three coumarin ibuprofen hybrid hit compounds by connecting diacylhydrazide (−CONHNHOC−), oxadiazole, and acylhydrazone (−CONHN=C−) with the coumarin backbone. Subsequently, we simulated a batch of lead compounds by introducing different substituents on the structure of coumarin using auto in silico ligand directing evolution (AILDE).[38−41] By calculating their binding energies with COX-2, we selected some promising compounds for synthesis. Through enzyme activity and cell experiments, we obtained two lead compounds with excellent activity against cervical cancer cells: **6c** (IC$_{50}$ = 0.606 μM, HeLa) and **7g** (IC$_{50}$ = 0.783 μM, HeLa). The calculation results also revealed that the two compounds are potential selective COX-2 inhibitors. We believe that our research will provide new ideas and a basis for exploring cancer chemotherapy methods targeting COX-2.

2. RESULTS AND DISCUSSION

2.1. Hit-to-Lead (H2L) Optimization. Based on the drug combination principle, bishydrazide, oxadiazole, and acylhydrazone (Figure S1) are selected as the linker groups to connect ibuprofen and coumarin to obtain three hit compounds **6a**, **7a**, and **8a** (Scheme 1). We performed the

calculation of AILDE to the H2L optimization of **6a**, **7a**, and **8a** to discover potent anticancer lead compounds. The AILDE protocol was developed by the author before as an in silico efficient and general approach for rapid identification of potent drug lead from hit compound.[38−41] AILDE performs minor chemical modifications on the scaffold of a hit compound, and these modifications can result in minimal losses or, in some cases, even increases in ligand efficiency. In this study, 9 most commonly used substituents (−Br, −CF$_3$, −CH$_3$, −Cl, −F, −NH$_2$, −NO$_2$, −OCH$_3$, and −OH) in current drugs were considered as minor modification groups to replace in the R position (5−8-position on the coumarin ring) of the three hit compounds (**6a**, **7a**, and **8a**). According to the docking and molecular dynamics (MD) simulation results of the three hit compounds with COX-2, the three hit compounds show a binding mode similar to that of COX-2 (Figure 1A). Both of
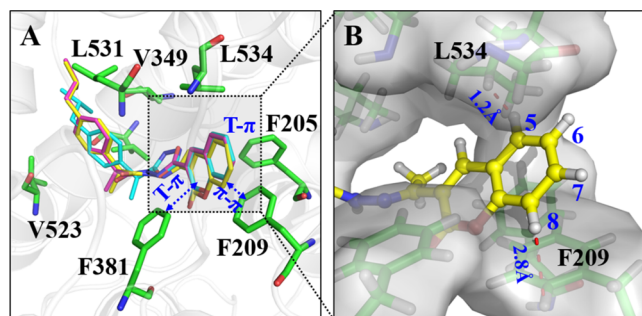

Figure 1. Simulated binding mode of hit compounds with COX-2. (A) The superimposition of modeled complex structures of COX-2 with **6a**, **7a**, and **8a**. **6a** is shown in yellow sticks, **7a** is shown in magenta sticks, and **8a** is shown in cyan sticks. The receptor (PDB ID: 5F1A) is shown in green sticks and white cartoons. (B) The binding mode of the R position on the coumarin ring of **6a** with COX-2. **6a** is the representative in the cavity for view and is shown with a yellow ball-and-stick model. COX-2 is shown with green sticks and a gray surface. The distances are shown with red dashed lines and labeled in blue font. The substitution positions on the coumarin ring are labeled with blue numbers.

them formed hydrophobic interactions with side chains of V349, L352, V523, and L531 by using the ibuprofen part. The coumarin part occupies the interior of the active cavity and forms π−π interaction with F209 and F381, T−π interaction with F205, and hydrophobic interaction with L534. By

analyzing the binding mode of hit compounds and COX-2, we found that the H atom on the 5-position of the coumarin ring was about 1.2 Å to the side chain of L534 (Figure 1B), which is a limited space for replacing an atom or a group with a larger radius than H. Therefore, we did not consider the group optimization on the 5-position. For the 6- and 7-position, it is observed that there is relatively enough space between hit compounds and COX-2 for the optimization of substituents (Figure 1B) so that the nine commonly used substituents were introduced to the two positions to generate new lead compounds. For the 8-position, its distance to the F209 (2.8 Å) can only accommodate one single atom, so we only consider replacing three halogen atoms (−Br, −Cl, −F) at the 8-position.

Based on the above analysis, we conducted ALIDE calculations on 6, 7, and 8-positions (where the 8-position only considers halogen substitution) of the coumarin ring. In addition to considering single substitution, we also calculated the compounds produced by disubstitution. We generated 156 potential lead compounds for each hit compound. The binding free energy shifts (ΔΔG) are calculated to evaluate the potential activity of new compounds. The calculated process is shown in Figure 2. A positive ΔΔG value indicated a decrease in the activity of the new compound compared to the hit compound, while a negative value indicated an increase in the activity of the new compound compared to the hit compound. Eighteen top-ranked and easily synthesizable compounds were synthesized for further bioassay tests. The structures of selected compounds with the calculated results are shown in Scheme 1 (For detailed structures, see Figure S2 in the Supporting Information).

2.2. Synthesis. According to the active substructure splicing principle and AILDE computational approaches, target compounds **6**, **7**, and **8** were prepared, and the routes are outlined in Scheme 1. First, following the reference method, from commercially available salicylic aldehyde, diethyl malonate, or ethyl acetoacetate, and other chemical reagents, the synthetic reactions of a series of substituted 3-acetyl-coumarin **3**, coumarin acyl chloride **4**, and ibuprofen-hydrazide **5** proceeded smoothly with satisfactory yields. Subsequently, compounds **6a−6g** were prepared using the reaction of **5** and different substituted 3-acetyl-coumarin **3** in the presence of AcOH-NaAc at 70−80 °C in good yields. In the presence of a slight excess of triethylamine as a catalyst, **4** and **5** were easily
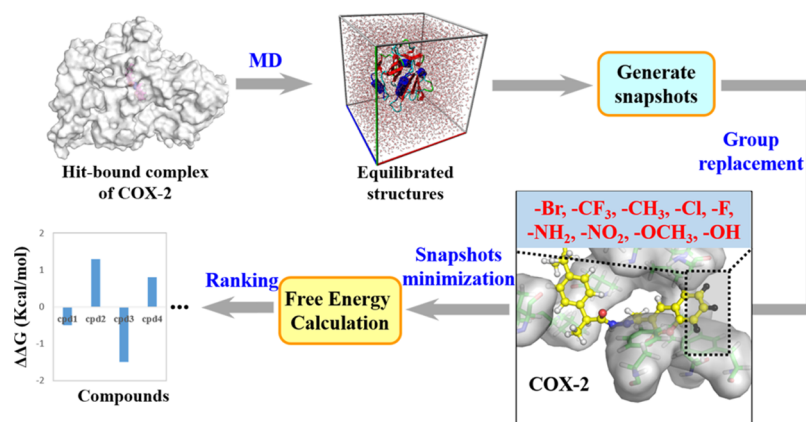

Figure 2. Calculation process of our study. It includes molecular dynamics (MD) simulation, AILDE, and free energy calculation. The detailed calculation methods are described in Section 4 and the Supporting Information.

converted to ibuprofen−coumarin bishydrazide hybrid derivatives 7a–7h in methylene dichloride at 0−5 °C. Finally, compounds 7 were further reacted with POCl$_3$ at 80−85 °C to produce the new target compounds 8a–8f. The results are displayed in Table 1. Compounds 6a–6g, 7a–7h, and 8a–8f were identified by ^{1}H and ^{13}C NMR and HRMS (ESI), and the proposed structures are consistent with all of the data.

Table 1. Structures and Cell-Based IC$_{50}$ (HeLa Cell) of Ibuprofen−Coumarin Hybrid Compounds with Calculated ($\Delta\Delta G_{cal}$) and Experimental ($\Delta\Delta G_{exp}$) Binding Free Energy Shift Compared to Hit Compounds 6a, 7a, and 8a

Cpds.	yield, %	cell-based IC$_{50}$ (HeLa, μM)	F^a	$\Delta\Delta G_{exp}$ (kcal mol^{-1})	$\Delta\Delta G_{cal}$ (kcal mol^{-1})
6a (Hit)	85	4.641	1.00	0.00	0.00
6b	66	2.588	1.78	−0.34	−0.27
6c	68	0.606	7.61	−1.21	−1.25
6d	64	6.650	0.69	0.22	0.31
6e	86	2.186	2.11	−0.44	−0.47
6f	67	4.344	1.06	−0.04	−0.28
6g	83	2.564	1.80	−0.35	−0.69
7a (Hit)	72	4.608	1.00	0.00	0.00
7b	84	42.693	0.11	1.33	0.17
7c	62	8.916	0.52	0.39	0.47
7d	85	136.56	0.03	2.02	0.53
7e	76	3.676	1.25	−0.13	−1.08
7f	64	6.246	0.74	0.18	0.81
7g	65	0.783	5.89	−1.06	−1.21
7h	75	0.889	5.18	−0.98	−2.51
8a (Hit)	62	4.659	1.00	0.00	0.00
8b	68	121.54	0.04	1.94	1.78
8c	75	82.163	0.06	1.71	0.31
8d	65	>200			1.06
8e	70	>200			1.08
8f	72	42.299	0.11	1.31	0.66
ibuprofen		>200			
gefitinib		5.285			

^{a}Activity fold compared to hit compounds, $F = $ IC$_{50}$(Hit)/IC$_{50}$(Lead)

2.3. Biological Evaluation.

To testify compounds as potential COX-2 inhibitors, 6 compounds (6c, 6d, 6f, 7a, 7e, 7f) were used to perform the enzyme-based activity test, and celecoxib was used as a reference drug with the IC$_{50}$ = 0.076 μM. As shown in Table 2, All 6 tested compounds have micromolar enzyme inhibitory activity against COX-2 with a range from 0.294 to 2.671 μM. 7e displayed moderate COX-2 inhibitory activity (IC$_{50}$ = 0.294 μM), which proved that our compound indeed has a certain inhibitory effect on COX-2. Then, the HeLa cells were chosen for cell-based activity testing

Table 2. Enzyme Activity Results of Representative Compounds

Cpds.	COX-2 (IC$_{50}$, μM)
6c	2.671
6d	1.043
6f	1.513
7a	2.824
7e	0.294
7f	0.982
celecoxib	0.076

due to their strong positive COX-2 expression.[42−45] All of the 18 synthesized compounds were subjected to cell-based antitumor activity in vitro by using standard 2-(2-methoxy-4-nitrophenyl)-3-(4-nitrophenyl)-5-(2,4-disulfophenyl)-2H-tetrazolium sodium salt (CCK8) assay, and gefitinib as the positive control (result shown in Table 1). The results show that 16 compounds (except 8d and 8e) have potential antitumor activities with the IC$_{50}$ values (HeLa cells) ranging from 0.606 to 121.54 μM. The activity values of most compounds are less than 10 μM, among which compounds 6c and 7g have the most excellent activity with IC$_{50}$ of 0.606 and 0.783 μM on HeLa cells, respectively. Their activities are better than those of ibuprofen and the commonly used antitumor drug gefitinib (∼10-fold activity improvement). We may observe that the overall activities of series 6 and 7 compounds are better than those of series 8, indicating that the skeleton structure of series 6 and 7 has more advantages in drug properties.

2.4. Binding Mode Analysis and Selectivity Study.

We chose the two compounds with the best activity, 6c (IC$_{50}$ = 0.606 μM) and 7g (IC$_{50}$ = 0.783 μM), as well as their lead compounds 6a (IC$_{50}$ = 4.641 μM) and 7a (IC$_{50}$ = 4.608 μM), to compare their interaction modes with those of COX-2. The binding modes were obtained from the AILDE calculation results (shown in Figure 3A,B,E,F). We can observe that four compounds exhibit extremely similar binding poses in the active pocket of COX-2. The coumarin ring is inserted into the bottom of the active cavity, and the ibuprofen fragment lies in the door of the active cavity. Comparing compounds 6a and 6c, we can see that their coumarin rings form T−π interactions with F381 and F205 and π−π interactions with F209. The difference between compounds 6a and 6c in their interaction with COX-2 is that the 6-position bromine atom (R = 6,8−2Br) on the coumarin ring of 6c forms two halogen bonds with the main chain of G533 and V228, enhancing the binding between 6c and COX-2, which was not observed in the binding of 6a to COX-2 (Figure 3A,B). This explains why the structural change of the compound from compound 6a to compound 6c can increase the activity of compound 6c. Similar to the cases of 6a and 6c, compound 7g has better activity than 7a because the R substituent of 7g (R = 6,8-2Cl) also forms halogen bonds with G533 and V228 (Figure 3E,F).

The expression of COX-2 is significantly upregulated in most cancer cells. In contrast, in normal cells, COX-2 is barely expressed, while the expression of COX-1 remains relatively stable and is crucial for maintaining normal cellular physiological functions. We conducted docking and MD experiments with compounds 6c and 7g on COX-1 (MD trajectories are shown in Figure S3 of the Supporting Information). By comparing the binding modes of the compounds with those of COX-1 and COX-2, we aim to assess the safety of these compounds in normal cells. We first used molecular docking to obtain the initial conformation of 6c and 7g binding to COX-1 and then performed a 4 ns' MD simulation based on the docking result, obtaining stable conformations of 6c and 7g binding to COX-1. First, by analyzing the binding mode of 6c with COX-1 (Figure 3C), we can see that compared with its binding mode with COX-2 (Figure 3B), the conformation of the F209 side chain at the bottom of the COX-1 cavity has a large angle deflection, and the active cavity space is compressed, which leads to 6c not fully penetrating the bottom of the COX-1 cavity and the coumarin ring undergoing an angle deflection, further causing a
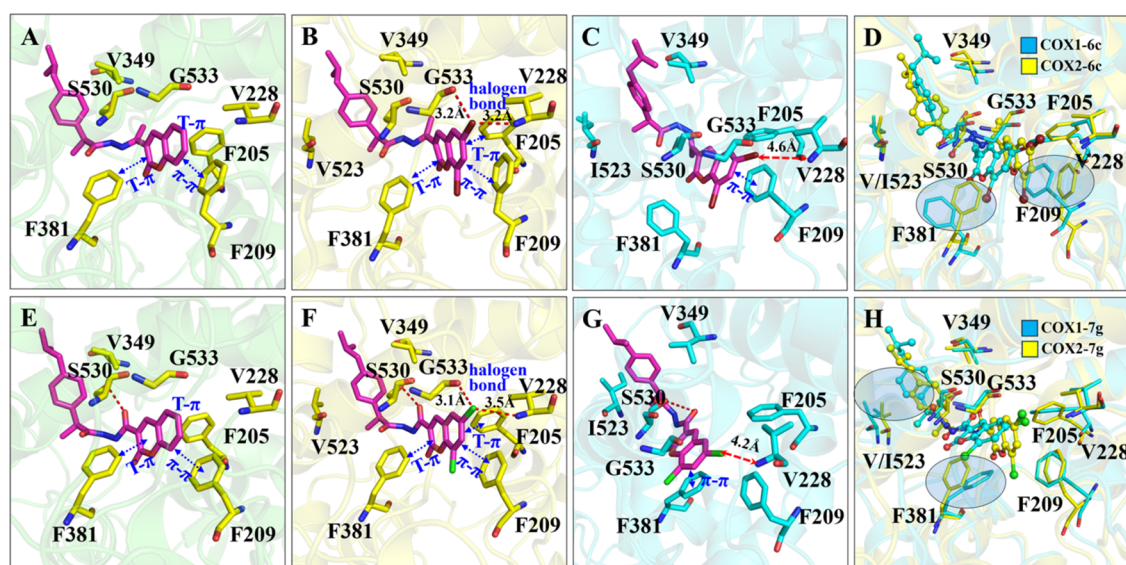
Figure 3. Predicted binding mode of compounds **6c** and **7g** with COX-1 and COX-2. (A) Binding mode of **6a** with COX-2. **6a** is shown as magenta sticks, and COX-2 is shown as yellow sticks and green cartoons. (B) The binding mode of **6c** with COX-2. **6c** is shown as magenta sticks, and COX-2 is shown as yellow sticks and cartoon. (C) The binding mode of **6c** with COX-1. **6c** is shown as magenta sticks, and COX-1 is shown as cyan sticks and cartoon. (D) Superimposition of **6c** with COX-2 and COX-1. The complexes formed by **6c** with COX-2 and COX-1 are colored yellow and cyan, respectively. (E) The binding mode of **7a** with COX-2. **7a** is shown as magenta sticks, and COX-2 is shown as yellow sticks and green cartoons. (F) The binding mode of **7g** with COX-2. **7g** is shown as magenta sticks, and COX-2 is shown as yellow sticks and cartoon. (G) The binding mode of **7g** with COX-1. **7g** is shown as magenta sticks, and COX-1 is shown as cyan sticks and cartoon. (H) Superimposition of **7g** with COX-2 and COX-1. The complexes formed by **7g** with COX-2 and COX-1 are shown in yellow and cyan, respectively.

Table 3. Calculated Binding Free Energies of Compound 6c and 7g with COX-1 and COX-2, Respectively

Cpds.	COX	binding free energies (kcal mol^{-1})[a]							predicted SI[b]
		ΔE_{ele}	ΔE_{vdW}	ΔE_{MM}	ΔG_{PB}	ΔG_{nP}	$-T\Delta S$	ΔG_{bind}	
6c	COX-1	−5.86	−66.18	−72.04	21.33	−8.01	12.45	−46.27	6.02
	COX-2	−7.46	−66.75	−74.22	22.44	−7.78	12.22	−47.34	
7g	COX-1	−6.11	−66.54	−72.63	22.01	−7.69	12.95	−45.36	5.09
	COX-2	−6.42	−65.50	−71.92	20.58	−7.58	12.59	−46.33	

[a]ΔE_{ele}, electrostatic energies; ΔE_{vdW}, van der Waals interaction; ΔE_{MM}: molecular mechanical (MM) gas-phase binding energy, which consists of ΔE_{ele} and ΔE_{vdW}; ΔG_{PB}: electrostatic contribution of solvation free energy; ΔG_{np}: nonelectrostatic of solvation free energy; $-T\Delta S$: entropic contribution; ΔG_{bind}: binding free energies, equals $\Delta E_{MM} + \Delta G_{PB} + \Delta G_{np} - T\Delta S$. [b]SI was calculated according to the equation $\Delta\Delta G_{bind} = \Delta G_{bind}(COX-2) - \Delta G_{bind}(COX-1) = -RT \ln SI$. For more details about the calculation method, see the Supporting Information.

conformational change in the F381 side chain (Figure 3D). This series of conformational changes results in the interaction between **6c** and COX-1 retaining only the $\pi-\pi$ interaction with F209, while the hydrophobic interactions with F381 and F205 are lost. The halogen bond interactions between the 6-position bromine atom on the coumarin ring with G533 and V288 are also lost due to improper distance or angle (Figure 3C,G), which ultimately leads to a weakening of the interaction between **6c** and COX-1 compared to that of COX-2. Upon further analysis of the interaction between **7g** and COX-1 (Figure 3G), we found that the conformational change of the F381 side chain in the cavity also caused the conformational deflection of the **7g** coumarin ring and the outward movement of the entire molecule, resulting in the loss of its interaction with F205 and F209, as well as the loss of its halogen bond interactions with G533 and V288 (Figure 3H). Due to the outward movement of the molecule, the ibuprofen fragment at the end of the molecule collided spatially with the I523 side chain at the entrance of the cavity, which also resulted in a weakening of the interaction between **7g** and COX-1 compared to that of COX-2.

We also used the MM-PBSA method[46] to calculate the binding free energies (ΔG_{bind}) of compounds **6c** and **7g** with COX-1 (detailed calculation method shown in the Supporting Information), and compared it with the binding free energies of compounds **6c** and **7g** with COX-2 obtained in the previous AILDE calculation (Table 3). We found that the binding free energy of compound **6c** with COX-2 is −47.34 kcal mol^{-1}, which is 1.07 kcal mol^{-1} stronger than its binding with COX-1 (−46.27 kcal mol^{-1}). Using the equation $\Delta\Delta G_{bind} = -RT \ln SI$, we can calculate the predicted selectivity index (SI) to be 6.02. From the energy component, we can see that the main reason for the difference in binding affinity is the electrostatic energies (ΔE_{ele}). The ΔE_{ele} value of compound 6c with COX-2 is −7.46 kcal mol^{-1}, which is 1.60 kcal mol^{-1} higher than its value with COX-1 (−5.86 kcal mol^{-1}). This is mainly due to the loss of halogen bonds of **6c** with COX-1 compared to its interaction with COX-2. Similarly, we obtained a selectivity index of 5.09 for **7g** through a computational prediction.

In summary, the different conformations of key amino acid residues in the COX-1 and COX-2 cavities lead to different binding modes of compounds, resulting in differences in

binding ability, allowing compounds to have better binding to COX-2, and ensuring that the compound has certain selectivity and safety. We have also quantitatively demonstrated this point through calculations and predicted that the two highly active compounds, **6c** and **7g**, are COX-2 selective inhibitors with SI of approximately 6-fold and 5-fold, respectively.

To clarify the selectivity of our compounds to cancer cells and normal cells, we also performed experiments and tested the proliferation inhibitory activity of compounds **6c** and **7g** on HEK293 cells, which is a cell line derived from human embryonic kidney cells. The results showed that the IC_{50} values of **6c** and **7g** on HEK293 cells were 32.230 and 19.960 μM, respectively. Comparing the inhibitory activities of the two compounds on HeLa cells, we can see that these two compounds exhibit 53.18- and 25.49-fold selectivity for cancer cells over normal cells, respectively (Table 4). The selectivity value demonstrates that our compounds possess an acceptable safety toward normal cells.

Table 4. Selectivity of Cell-based Activity of Compounds 6c and 7g toward Cancer Cells (HeLa) and Normal Cells (HEK293)

Cpds.	cell-based IC_{50} (HeLa, μM)	cell-based IC_{50} (HEK293, μM)	SI[a]
6c	0.606	32.230	53.18
7g	0.783	19.960	25.49

[a]SI = IC_{50}(HEK293)/IC_{50}(HeLa).

3. CONCLUSIONS

In this study, we used the cyclooxygenase inhibitor ibuprofen as the precursor and synthesized three ibuprofen−coumarin hybrid hit compounds by connecting diacylhydrazide, oxadiazole, and acylhydrazone to the coumarin backbone. To obtain more potential antitumor active compounds, we employed the computational AILDE method for rational structure optimization from hit-to-lead. We ultimately designed and synthesized 18 ibuprofen−coumarin derivatives targeting COX-2, among which compounds **6c** (IC_{50} = 0.606 μM, HeLa) and **7g** (IC_{50} = 0.783 μM, HeLa) exhibited excellent activity against cervical cancer cells. The calculation results and cell-based activity assay demonstrated that they have potential selectivity for COX-2. The novel compound structures discovered in this study provide new ideas for the research of anticancer drugs targeting COX-2.

4. MATERIALS AND METHODS

4.1. Computational Methods. *4.1.1. Molecular Docking and MD Simulation.* The three-dimensional (3D) structures were prepared by SYBYL 7.0. Structures of COX-1 (PDB ID: 6Y3C)[47] and COX-2 (PDB ID: 5F1A)[48] were downloaded from the RCSB Protein Data Bank (PDB, https://www.rcsb.org/).[49] The hydrogens of the receptor were added using Discovery Studio 4.0. The GOLD 3.0 was used to dock compounds into the active center. MD simulation was performed using Amber16. More description of the computational settings can be seen in the Supporting Information.

4.1.2. AILDE. Fifty snapshots were extracted from the last 500 ps of the MD trajectory with a time step of 10 ps by using the Cpptraj module in the Amber16 program. We introduced different small groups (−Br, −CF$_3$, −CH$_3$, −Cl, −F, −NH$_2$, −NO$_2$, −OCH$_3$, and −OH) to replace hydrogen atoms of **6a**,

7a, and **8a** in the snapshots by using a modified version of AutoGrow.[50] Because the growth algorithm started from the hit compound placed in the binding site and was based on the binding conformation, a series of new compounds bound to the receptor were generated as lead compounds. Then, we minimized the complex structure to obtain the final structures of the newly generated lead−receptor complexes. First, we minimized all side chain atoms of the receptor and fixed the receptor backbone and lead compound. Second, we minimized the complex, allowing all of the atoms to move. Both steps were a combination of the 2000-step steepest descent method and the 2000-step conjugated gradient method with a convergence criterion of 0.2 kcal mol^{-1}. Each snapshot of the lead−receptor complex was dealt with using the same minimization strategies to maintain parallel processes.

4.1.3. Free Energy Calculation. The MM-PBSA method was used to calculate the binding free energy (ΔG_{bind}) between the receptor and the ligand.[46] This value was obtained by calculating the differences in free energies between the ligand−receptor complex (G_{cpx}) and the unbound receptor (G_{rec}) and ligand (G_{lig}) as follows

$$\Delta G_{bind} = G_{cpx} - (G_{rec} + G_{lig}) \tag{1}$$

The binding free energy shift ($\Delta\Delta G_{cal}$) between the hit−receptor and lead−receptor complex is defined as follows

$$\Delta\Delta G_{cal} = \Delta G_{bind}(\text{Lead}) - \Delta G_{bind}(\text{Hit}) \tag{2}$$

$\Delta\Delta G$ was used to evaluate the change in the binding affinity after group replacement. A positive $\Delta\Delta G$ value indicates a decrease in the binding affinity, and a negative value represents an increase in the binding affinity. $\Delta\Delta G$ was also used to predict the selectivity index (SI) value in our study according to the following equation[51−53]

$$\Delta\Delta G_{bind} = \Delta G_{bind}(\text{COX-2}) - \Delta G_{bind}(\text{COX-1})$$
$$= -RT\ln \text{SI} \tag{3}$$

For more information on the principles and methods of binding free energy calculation in this study, see the Supporting Information.

4.2. Chemistry Section. *4.2.1. General.* Mp was measured on an uncorrected X-4 digital melting point apparatus. ^{1}H and ^{13}C NMR were recorded on a Bruker Avance 400 MHz spectrometer (CDCl$_3$ and DMSO-d_6) with resonances relative to tetramethylsilane (TMS) as an internal standard. Mass spectra (ESI) were recorded on a Waters XEVO G2-XS mass spectrometer. Unless otherwise stated, starting materials, reagents, and solvents used in this experiment were commercially available (analytically pure) and used without further purification. TLC analysis was performed on silica gel plates GF254 (Wuhan, Geao Co.).

4.2.2. Synthesis Procedure for Compounds 6a−6g. Intermediates **2**, **3**, **4**, and **5** were generally prepared according to the literature procedures and an approach similar to those previously reported. A mixture of substituted 3-acetyl-coumarin **3** (5 mmol), ibuprofen-hydrazide **5** (5.2 mmol), and AcOH (10 mL) was refluxed. The completion of the reaction was monitored by TLC, the reaction mixture was poured into crushed ice to precipitate the product and was filtered, and the crude product was further recrystallized from CH$_2$Cl$_2$/EtOH to provide compounds **6a−6g**.

4.2.2.1. (E)-2-(4-Isobutylphenyl)-N′-(1-(2-oxo-2H-chromen-3-yl)ethylidene)propanehydrazide (6a). White solid.

Mp: 111−113 °C; ^{1}H NMR (400 MHz, CDCl$_3$) δ: 8.85 and 8.33 (s, 1H, NH and OH, keto−enol tautomerism, keto-(−CONH−)/enol(−HOC=N−) ratio 34/66), 8.14 and 7.68 (s, 1H, H-4 coumarin), 7.59−7.12 (m, 8H, ArH), 4.57−4.55 and 3.78−3.76 (m, 1H, CH), 2.50−2.47 (m, 2H, CH$_2$), 2.18 and 1.91 (s, 3H, CH$_3$), 1.89−1.83 (m, 1H, CH), 1.66 and 1.51 (d, J = 8.0 Hz, 3H, CH$_3$), 0.91 (d, J = 4.0 Hz, 6H, 2 × CH$_3$); ^{13}C NMR (100 MHz, CDCl$_3$) δ: 176.31, 159.95, 154.03, 144.68, 141.41, 140.22, 138.94, 132.29, 130.10, 129.30, 128.47, 127.58, 124.76, 119.08, 116.63, 45.12, 41.98, 30.26, 22.46, 22.32, 18.79; HRMS (ESI) m/z: Anal. calcd for C$_{24}$H$_{27}$N$_2$O$_3$ [M + H]$^+$: 391.2022, found: 391.2025 (M$^+$, 100); anal. RP-UPLC t_R(keto) = 24.710 min, t_R(enol) = 26.277 min, purity 99.55%, UV 330 nm.

4.2.2.2. (E)-N′-(1-(6-Fluoro-2-oxo-2H-chromen-3-yl)-ethylidene)-2-(4-isobutylphenyl)propanehydrazide (6b). Yellow solid. Mp: 186−187 °C; ^{1}H NMR (400 MHz, CDCl$_3$) δ: 8.67 and 8.34 (s, 1H, NH and OH, keto−enol tautomerism, keto(−CONH−)/enol(−HOC=N−) ratio 33/67), 8.08 and 7.57 (s, 1H, H-4 coumarin), 7.33−7.12 (m, 7H, ArH), 4.56−4.51 and 3.78−3.76 (m, 1H, CH), 2.48 (d, J = 8.0 Hz, 2H, CH$_2$), 2.17 and 1.90 (s, 3H, CH$_3$), 1.89−1.84 (m, 1H, CH), 1.66 and 1.51 (d, J = 8.0 Hz, 3H, CH$_3$), 0.91 (d, J = 4.0 Hz, 6H, 2 × CH$_3$); ^{13}C NMR (100 MHz, CDCl$_3$) δ: 176.32, 160.09, 157.65, 150.18, 140.29, 138.94, 130.12, 129.33, 127.85, 127.52, 199.83, 118.23, 118.15, 113.66, 113.42, 45.10, 42.09, 30.24, 22.44, 18.83, 14.21; HRMS (ESI) m/z: Anal. calcd for C$_{24}$H$_{26}$FN$_2$O$_3$ [M + H]$^+$: 409.1927, found: 409.1931 (M$^+$, 100); anal. RP-UPLC t_R(keto) = 25.147 min, t_R(enol) = 26.788 min, purity 99.62%, UV 330 nm.

4.2.2.3. (E)-N′-(1-(6,8-Dibromo-2-oxo-2H-chromen-3-yl)-ethylidene)-2-(4-isobutylphenyl)propanehydrazide (6c). White solid. Mp: 206−207 °C; ^{1}H NMR (400 MHz, CDCl$_3$) δ: 8.92 and 8.43 (s, 1H, NH and OH, keto−enol tautomerism, keto(−CONH−)/enol(−HOC=N−) ratio 30/70), 8.00 and 7.89 (s, 1H, H-4 coumarin), 7.59−7.11 (m, 7H, ArH), 4.53−4.48 and 3.78−3.76 (m, 1H, CH), 2.49 (d, J = 8.0 Hz, 2H, CH$_2$), 2.18 and 1.90 (s, 3H, CH$_3$), 1.89−1.85 (m, 1H, CH), 1.66 and 1.50 (d, J = 4.0 Hz, 3H, CH$_3$), 0.91−0.90 (m, 6H, 2 × CH$_3$); ^{13}C NMR (100 MHz, CDCl$_3$) δ: 176.45, 158.29, 149.79, 143.68, 140.22, 139.49, 139.02, 137.51, 130.12, 129.90, 129.36, 127.47, 121.36, 117.14, 111.09, 45.11, 42.23, 30.24, 22.44, 18.89, 14.21; HRMS (ESI) m/z: Anal. calcd for C$_{24}$H$_{25}$Br$_2$N$_2$O$_3$ [M + H]$^+$: 547.0232, found: 547.0235 (M$^+$, 100); anal. RP-UPLC t_R = 30.123 min, purity 99.54%, UV 330 nm.

4.2.2.4. (E)-N′-(1-(7-Hydroxy-2-oxo-2H-chromen-3-yl)-ethylidene)-2-(4-isobutylphenyl)propanehydrazide (6d). Yellow solid. Mp: 125−127 °C; ^{1}H NMR (400 MHz, CDCl$_3$) δ: 9.77 (s, 1H, Ar−OH), 8.70 and 8.53 (s, 1H, NH and OH, keto−enol tautomerism, keto(−CONH−)/enol(−HOC=N−) ratio 20/80), 7.63 and 7.31 (s, 1H, H-4 coumarin), 7.29−6.96 (m, 7H, ArH), 3.85−3.80 and 3.76−3.71 (m, 1H, CH), 2.49 (d, J = 8.0 Hz, 2H, CH$_2$), 2.16 and 1.92 (s, 3H, CH$_3$), 1.87−1.84 (m, H, CH), 1.68 and 1.50 (d, J = 8.0 Hz, 3H, CH$_3$), 0.89 (d, J = 8.0 Hz, 6H, 2 × CH$_3$); ^{13}C NMR (100 MHz, CDCl$_3$) δ: 172.54, 161.90, 160.42, 155.36, 152.20, 142.57, 141.79, 136.76, 130.13, 129.73, 127.58, 120.58, 114.34, 110.93, 103.46, 45.68, 44.98, 30.23, 22.31, 18.04, 14.69; HRMS (ESI) m/z: Anal. calcd for C$_{24}$H$_{27}$N$_2$O$_4$ [M + H]$^+$: 407.1971, found: 407.1970 (M$^+$, 100); anal. RP-UPLC t_R(keto) = 22.742 min, t_R(enol) = 23.904 min, purity 99.40%, UV 330 nm.

4.2.2.5. (E)-2-(4-Isobutylphenyl)-N′-(1-(6-methyl-2-oxo-2H-chromen-3-yl)ethylidene)propanehydrazide (6e). White solid. Mp: 168−170 °C; ^{1}H NMR (400 MHz, CDCl$_3$) δ: 8.81 and 8.37 (s, 1H, NH and OH, keto−enol tautomerism, keto(−CONH−)/enol(−HOC=N−) ratio 32/68), 8.07 and 7.61 (s, 1H, H-4 coumarin), 7.38−7.12 (m, 7H, ArH), 4.60−4.54 and 3.78−3.76 (m, 1H, CH), 2.49−2.47 (m, 2H, CH$_2$), 2.45−2.39 (m, 3H, CH$_3$), 2.19 and 1.91 (s, 3H, CH$_3$), 1.88−1.83 (m, 1H, CH), 1.66 and 1.51 (d, J = 8.0 Hz, 3H, CH$_3$), 0.91 (d, J = 8.0 Hz, 6H, 2 × CH$_3$); ^{13}C NMR (100 MHz, CDCl$_3$) δ: 178.44, 160.18, 152.19, 145.00, 141.44, 140.13, 138.98, 134.43, 133.35, 130.08, 129.29, 127.59,. 126.66, 118.82, 116.31, 45.14, 41.92, 30.25, 22.48, 20.83, 18.79, 14.40; HRMS(ESI) m/z: Anal. calcd for C$_{25}$H$_{29}$N$_2$O$_3$ [M + H]$^+$: 405.2178, found: 405.2181 (M$^+$, 100); anal. RP-UPLC t_R(keto) = 25.734 min, t_R(enol) = 27.580 min, purity 98.55%, UV 330 nm.

4.2.2.6. (E)-N′-(1-(6,8-Dichloro-2-oxo-2H-chromen-3-yl)-ethylidene)-2-(4-isobutylphenyl)propanehydrazide (6f). White solid. Mp: 180−182 °C; ^{1}H NMR (400 MHz, CDCl$_3$) δ: 8.66 and 8.35 (s, 1H, NH and OH, keto−enol tautomerism, keto(−CONH−)/enol(−HOC=N−) ratio 34/66), 8.04 and 7.61 (s, 1H, H-4 coumarin), 7.47−7.12 (m, 7H, ArH), 4.53−4.48 and 3.78−3.76 (m, 1H, CH), 2.49 (d, J = 4.0 Hz, 2H, CH$_2$), 2.17 and 1.90 (s, 3H, CH$_3$), 1.90−1.87 (m, 1H, CH), 1.66 and 1.51 (d, J = 8.0 Hz, 3H, CH$_3$), 0.91−0.90 (d, J = 4.0 Hz, 6H, 2 × CH$_3$); ^{13}C NMR (100 MHz, CDCl$_3$) δ: 176.24, 148.27, 139.60, 132.22, 132.06, 130.16, 129.91, 129.37, 128.50, 127.47, 126.50, 126.15, 122.53, 120.89, 104.48, 45.09, 42.22, 30.25, 22.45, 18.89, 14.05; HRMS (ESI) m/z: Anal. calcd for C$_{24}$H$_{25}$Cl$_2$N$_2$O$_3$ [M + H]$^+$: 459.1242, found: 459.1246 (M$^+$, 100); anal. RP-UPLC t_R(keto) = 27.339 min, t_R(enol) = 29.455 min, purity 99.55%, UV 330 nm.

4.2.2.7. (E)-N′-(1-(6-Chloro-2-oxo-2H-chromen-3-yl)-ethylidene)-2-(4-isobutylphenyl)propanehydrazide (6g). White solid. Mp: 169−171 °C; ^{1}H NMR (400 MHz, CDCl$_3$) δ: 8.65 and 8.42 (s, 1H, NH and OH, keto−enol tautomerism, keto(−CONH−)/enol(−HOC=N−) ratio 29/71), 8.33 and 8.05 (s, 1H, H-4 coumarin), 7.64−7.13 (m, 7H, ArH), 4.55−4.50 and 3.78−3.76 (m, 1H, CH), 2.49 (d, J = 8.0 Hz, 2H, CH$_2$), 2.17 and 1.90 (s, 3H, CH$_3$), 1.87−1.84 (m, 1H, CH), 1.66 and 1.51 (d, J = 8.0 Hz, 3H, CH$_3$), 0.91 (d, J = 8.0 Hz, 6H, 2 × CH$_3$); ^{13}C NMR (100 MHz, CDCl$_3$) δ: 176.28, 159.33, 152.34, 144.08, 140.04, 138.96, 134.28, 132.13, 130.00, 129.35, 127.81, 127.62, 127.50, 120.10, 118.20, 118.02, 30.25, 22.45, 18.85, 17.99, 14.18; HRMS (ESI) m/z: Anal. calcd for C$_{24}$H$_{26}$ClN$_2$O$_3$ [M + H]$^+$: 425.1632, found: 425.1636 (M$^+$, 100); anal. RP-UPLC t_R(keto) = 19.105 min, t_R(enol) = 28.065 min, purity 96.19%, UV 330 nm.

4.2.3. Synthesis Procedure for Compounds 7a−7i. To a stirred mixture of **5** (5 mmol) and **4** (5 mmol) in dry CH$_2$Cl$_2$ (20 mL) was slowly added triethylamine (6−8 mmol) and allowed to stand for 10−12 h at ice bath conditions, then concentrated and poured into ice water. The solid was filtered and washed well with a water/ethanol solution. the product was purified by recrystallization in CH$_2$Cl$_2$/C$_2$H$_5$OH (v/v = 1:2) to afford the desired compounds **7a−7i**.

4.2.3.1. N′-(2-(4-Isobutylphenyl)propanoyl)-2-oxo-2H-chromene-3-carbohydrazide (7a). White solid. Mp: 200−202 °C; ^{1}H NMR (400 MHz, DMSO-d_6) δ: 11.07 (s, 1H, NH), 10.73 (s, 1H, NH), 8.90 (s, 1H, H-4 coumarin), 8.04−7.11 (m, 8H, ArH), 3.84−3.83 (m, 1H, CH), 2.42 (d, J = 8.0 Hz, 2H, CH$_2$), 1.85−1.80 (m, 1H, CH), 1.41 (d, J = 4.0 Hz,

3H, CH$_3$), 0.87 (d, J = 8.0 Hz, 6H, 2 × CH$_3$); ^{13}C NMR (100 MHz, DMSO-d_6) δ: 170.69, 159.87, 158.14, 153.89, 147.79, 139.49, 138.58, 134.37, 130.31, 128.81, 127.08, 125.23, 118.29, 118.02, 116.23, 44.23, 42.19, 29.81, 22.18, 18.42; HRMS (ESI) m/z: Anal. calcd for C$_{23}$H$_{25}$N$_2$O$_4$ [M + H]$^+$: 393.1814, found: 393.1833 (M$^+$, 100); anal. RP-UPLC t_R = 24.588 min, purity 97.48%, UV 330 nm.

4.2.3.2. N′-(2-(4-Isobutylphenyl)propanoyl)-6-methyl-2-oxo-2H-chromene-3-carbohydrazide (7b). White solid. Mp: 206−208 °C; ^{1}H NMR (400 MHz, CDCl$_3$) δ: 11.18 (d, J = 8.0 Hz, 1H, NH), 9.04 (d, J = 8.0 Hz, 1H, NH), 8.73 (s, 1H, H-4 coumarin), 7.49−7.10 (m, 7H, ArH), 3.77−3.72 (m, 1H, CH), 2.45−2.41 (m, 4H, 1 × CH 1 × CH$_3$), 1.87−1.81 (m, 1H, CH), 1.58 (d, J = 8.0 Hz, 3H, CH$_3$), 0.89 (d, J = 8.0 Hz, 6H, 2 × CH$_3$); ^{13}C NMR (100 MHz, CDCl$_3$) δ: 170.64, 160.70, 157.77, 152.72, 148.69, 140.99, 137.44, 135.83, 135.39, 129.66, 129.44, 127.39, 118.07, 116.66, 116.57, 45.05, 44.60, 30.18, 22.42, 20.77, 18.55; HRMS (ESI) m/z: Anal. calcd for C$_{24}$H$_{27}$N$_2$O$_4$ [M + H]$^+$: 407.1971, found: 407.1970 (M$^+$, 100); anal. RP-UPLC t_R = 25.447 min, purity 97.19%, UV 330 nm.

4.2.3.3. 7-Hydroxy-N′-(2-(4-isobutylphenyl)propanoyl)-2-oxo-2H-chromene-3-carbohydrazide (7c). Yellow-green solid. Mp: 224−226 °C; ^{1}H NMR (400 MHz, CDCl$_3$) δ: 11.02 (s, 1H, NH), 10.63 (s, 1H, NH), 8.82 (s, 1H, H-4 coumarin), 7.96−6.82 (m, 7H, ArH), 3.82 (t, J = 8.0 Hz, 1H, CH), 2.41 (m, 2H, 1 × CH$_2$), 1.84−1.79 (m, 1H, CH), 1.39 (d, J = 8.0 Hz, 3H, CH$_3$), 0.86 (d, J = 8.0 Hz, 6H, 2 × CH$_3$); ^{13}C NMR (100 MHz, DMSO-d_6) δ: 170.58, 164.50, 162.28, 160.65, 158.67, 156.45, 148.46, 139.45, 138.60, 132.09, 128.78, 127.07, 114.69, 110.84, 101.90, 44.23, 42.16, 29.16, 22.16, 18.41; HRMS (ESI) m/z: Anal. calcd for C$_{23}$H$_{25}$N$_2$O$_5$ [M + H]$^+$: 409.1763, found: 409.1764 (M$^+$, 100); anal. RP-UPLC t_R = 22.876 min, purity 96.05%, UV 330 nm.

4.2.3.4. 6-Chloro-N′-(2-(4-isobutylphenyl)propanoyl)-2-oxo-2H-chromene-3-carbohydrazide (7d). White solid. Mp: 206−208 °C; ^{1}H NMR (400 MHz, CDCl$_3$) δ: 11.05 (d, J = 4.0 Hz, 1H, NH), 8.74 (s, 1H, NH), 8.40 (d, J = 8.0 Hz, 1H, H-4 coumarin), 7.65−7.13 (m, 7H, ArH), 3.71 (q, J = 8.0 Hz, 1H, CH), 2.46 (d, J = 8.0 Hz, 2H, CH$_2$), 1.89−1.82 (m, 1H, CH), 1.61−1.58 (m, 3H, CH$_3$), 0.91 (d, J = 8.0 Hz, 6H, 2 × CH$_3$); ^{13}C NMR (100 MHz, CDCl$_3$) δ: 170.53, 159.93, 157.07, 152.81, 147.47, 141.26, 137.07, 134.51, 130.90, 129.82, 128.82, 127.40, 119.24, 118.36, 117.95, 45.04, 44.88, 30.19, 22.42, 18.44; HRMS (ESI) m/z: Anal. calcd for C$_{23}$H$_{24}$ClN$_2$O$_4$ [M + H]$^+$: 427.1425, found: 427.1424 (M$^+$, 100); anal. RP-UPLC t_R = 25.773 min, purity 96.37%, UV 330 nm.

4.2.3.5. 6-Fluoro-N′-(2-(4-isobutylphenyl)propanoyl)-2-oxo-2H-chromene-3-carbohydrazide (7e). White solid. Mp: 200−203 °C; ^{1}H NMR (400 MHz, DMSO-d_6) δ: 11.07 (s, 1H, NH), 10.73 (s, 1H, NH), 8.85 (s, 1H, H-4 coumarin), 7.92−7.09 (m, 7H, ArH), 3.81 (q, J = 8.0 Hz, 1H, CH), 2.41 (d, J = 8.0 Hz, 2H, CH$_2$), 1.84−1.77 (m, 1H, CH), 1.38 (d, J = 8.0 Hz, 3H, CH$_3$), 0.84 (d, J = 8.0 Hz, 6H, 2 × CH$_3$); ^{13}C NMR (100 MHz, DMSO-d_6) δ: 170.68, 159.57, 157.89, 150.32, 146.69, 139.49, 138.55, 128.81, 127.07, 119.19, 118.39, 118.30, 115.26, 115.01, 99.49, 44.22, 42.18, 29.61, 22.17, 18.42; HRMS (ESI) m/z: Anal. calcd for C$_{23}$H$_{24}$FN$_2$O$_4$ [M + H]$^+$: 411.1720, found: 411.1722 (M$^+$, 100); anal. RP-UPLC t_R = 24.828 min, purity 98.92%, UV 330 nm.

4.2.3.6. N′-(2-(4-Isobutylphenyl)propanoyl)-6-nitro-2-oxo-2H-chromene-3-carbohydrazide (7f). Yellow solid. Mp: 212−215 °C; ^{1}H NMR (400 MHz, DMSO-d_6) δ: 11.02 (s, 1H, NH), 10.63 (s, 1H, NH), 9.01−7.10 (m, 8H, ArH), 3.80 (q, J = 8.0 Hz, 1H, CH), 2.41 (d, J = 8.0 Hz, 2H, CH$_2$), 1.84−1.79 (m, 1H, CH), 1.39 (d, J = 4.0 Hz, CH$_3$), 0.86 (d, J = 4.0 Hz, 6H, 2 × CH$_3$); ^{13}C NMR (100 MHz, DMSO-d_6) δ: 170.89, 158.78, 157.91, 157.30, 146.41, 143.94, 139.51, 138.54, 128.82, 128.31, 127.08, 126.00, 120.44, 118.68, 117.84, 44.22, 42.24, 29.61, 22.16, 18.41; HRMS (ESI) m/z: Anal. calcd for C$_{23}$H$_{24}$N$_3$O$_6$ [M + H]$^+$: 438.1665, found 438.1665 (M$^+$, 100); anal. RP-UPLC t_R = 24.938 min, purity 99.64%, UV 330 nm.

4.2.3.7. 6,8-Dichloro-N′-(2-(4-isobutylphenyl)propanoyl)-2-oxo-2H-chromene-3-carbohydrazide (7g). Yellow solid. Mp: 212−215 °C; ^{1}H NMR (400 MHz, DMSO-d_6) δ: 11.05 (s, 1H, NH), 10.64 (s, 1H, NH), 8.83 (s, 1H, H-4 coumarin), 8.15−7.10 (m, 6H, ArH), 3.80 (q, J = 8.0 Hz, 1H, CH), 2.42 (d, J = 8.0 Hz, 2H, CH$_2$), 1.85−1.80 (m, 1H, CH), 1.40 (d, J = 8.0 Hz, 3H, CH$_3$), 0.87 (d, J = 4.0 Hz, 6H, 2 × CH$_3$); ^{13}C NMR (100 MHz, DMSO-d_6) δ: 170.82, 158.47, 157.73, 148.32, 146.10, 139.50, 138.52, 132.95, 128.81, 128.74, 128.20, 127.08 120.88, 120.74, 120.31, 44.22, 42.21, 29.61, 22.16, 18.41; HRMS (ESI) m/z: Anal. calcd for C$_{23}$H$_{23}$Cl$_2$N$_2$O$_4$ [M + H]$^+$: 461.1035, found: 461.1034 (M$^+$, 100); anal. RP-UPLC t_R = 26.959 min, purity 99.15%, UV 330 nm.

4.2.3.8. 6,8-Dibromo-N′-(2-(4-isobutylphenyl)propanoyl)-2-oxo-2H-chromene-3-carbohydrazide (7h). White solid. Mp: 203−205 °C; ^{1}H NMR (400 MHz, CDCl$_3$) δ: 10.09 (s, 1H, NH), 8.69 (s, 1H, H-4 coumarin), 8.27 (s, 1H, NH), 8.02−7.14 (m, 6H, ArH), 3.70 (q, J = 8.0 Hz, 1H, CH), 2.46 (d, J = 8.0 Hz, 2H, CH$_2$), 1.89−1.82 (m, 1H, CH), 1.60 (d, J = 4.0 Hz, 3H, CH$_3$), 0.91 (d, J = 4.0 Hz, 6H, 2 × CH$_3$); ^{13}C NMR (100 MHz, CDCl$_3$) δ: 170.63, 158.98, 156.70, 150.28, 147.13, 141.32, 139.84, 136.99, 131.09, 129.86, 127.42, 120.45, 118.62, 118.06, 111.49, 45.04, 44.96, 30.19, 22.42, 18.40; HRMS (ESI) m/z: Anal. calcd for C$_{23}$H$_{23}$Br$_2$N$_2$O$_4$ [M + H]$^+$: 549.0025, found: 549.0024 (M$^+$, 100), anal. RP-UPLC t_R = 27.975 min, purity 95.15%, UV 330 nm.

4.2.4. Synthesis Procedure for Compounds 8a−8f. A suspension mixture of 7 (5 mmol) and phosphorus oxychloride (2 mL) was stirred at 90−95 °C for 7−8 h. The solution was concentrated under reduced pressure to remove excessive phosphorus oxychloride. The residue was poured into ice water and recrystallized from CH$_2$Cl$_2$/C$_2$H$_5$OH (v/v = 1:2) to give compounds 8a−8f.

4.2.4.1. 3-(5-(1-(4-Isobutylphenyl)ethyl)-1,3,4-oxadiazol-2-yl)-2H-chromen-2-one (8a). White solid. Mp:119−121 °C; ^{1}H NMR (400 MHz, CDCl$_3$) δ: 8.53 (s, H, H-4 coumarin), 7.66−7.11 (m, 8H, ArH), 4.46 (q, J = 8.0 Hz, H, CH), 2.45 (d, J = 4.0 Hz, 2H, CH$_2$), 1.87−1.84 (m, 1H, CH), 1.82 (d, J = 8.0 Hz, 3H, CH$_3$), 0.89 (d, J = 8.0 Hz, 6H, 2 × CH$_3$); ^{13}C NMR (100 MHz, CDCl$_3$) δ: 170.06, 161.01, 156.29, 154.60, 144.81, 141.12, 137.26, 134.02, 129.66, 129.19, 127.10, 125.16, 118.03, 116.95, 112.88, 45.03, 37.18, 30.15, 22.38, 19.73; HRMS (ESI) m/z: Anal. calcd for C$_{23}$H$_{23}$N$_2$O$_3$ [M + H]$^+$: 375.1709, found: 375.1709 (M$^+$, 100); anal. RP-UPLC t_R = 26.348 min, purity 99.49%, UV 330 nm.

4.2.4.2. 6-Fluoro-3-(5-(1-(4-isobutylphenyl)ethyl)-1,3,4-oxadiazol-2-yl)-2H-chromen-2-one (8b). White solid. Mp: 183−185 °C; ^{1}H NMR (400 MHz, CDCl$_3$) δ: 8.48 (s, H, H-4 coumarin), 7.39−7.11 (m, 7H, ArH), 4.46 (q, J = 8.0 Hz, H, CH), 2.45 (d, J = 4.0 Hz, 2H, CH$_2$), 1.87−1.86 (m, 1H, CH), 1.82 (d, J = 8.0 Hz, 3H, CH$_3$), 0.89 (d, J = 8.0 Hz, 6H, 2 × CH$_3$); ^{13}C NMR (100 MHz, CDCl$_3$) δ: 170.28, 160.70, 155.89, 150.75, 143.68, 141.18, 137.14,.129.68, 127.10, 121.69, 121.45, 118.67, 118.59, 114.31, 114.07, 45.02, 37.18, 30.17, 22.38, 19.70; HRMS (ESI) m/z: Anal. calcd for C$_{23}$H$_{22}$FN$_2$O$_3$

$[M + H]^+$: 393.1614, found: 393.1613 (M^+, 100); anal. RP-UPLC t_R = 26.713 min, purity 99.27%, UV 330 nm.

4.2.4.3. 6-Chloro-3-(5-(1-(4-isobutylphenyl)ethyl)-1,3,4-oxadiazol-2-yl)-2H-chromen-2-one (8c). White solid. Mp: 182−183 °C; ^{1}H NMR (400 MHz, CDCl$_3$) δ: 8.48 (s, H, H-4 coumarin), 7.60−7.11 (m, 7H, ArH), 4.46 (q, J = 8.0 Hz, H, CH), 2.45 (d, J = 4.0 Hz, 2H, CH$_2$), 1.87−1.84 (m, 1H, CH), 1.82 (d, J = 8.0 Hz, 3H, CH$_3$), 0.89 (d, J = 8.0 Hz, 6H, 2 × CH$_3$); ^{13}C NMR (100 MHz, CDCl$_3$) δ: 170.28, 160.63, 155.86, 152.89, 143.36, 141.19, 137.11, 133.89, 130.56, 129.68, 128.18, 127.10, 118.96, 118.40, 113.98, 45.02, 37.18, 30.17, 22.39, 19.89; HRMS (ESI) m/z: Anal. calcd for C$_{23}$H$_{22}$ClN$_2$O$_3$ $[M + H]^+$: 409.1319, found: 409.1322 (M^+, 100); anal. RP-UPLC t_R = 27.959 min, purity 99.20%, UV 330 nm.

4.2.4.4. 6,8-Dichloro-3-(5-(1-(4-isobutylphenyl)ethyl)-1,3,4-oxadiazol-2-yl)-2H-chromen-2-one (8d). White solid. Mp: 189−190 °C; ^{1}H NMR (400 MHz, CDCl$_3$) δ: 8.45 (s, H, H-4 coumarin), 7.69−7.12 (m, 6H, ArH), 4.46 (q, J = 8.0 Hz, H, CH), 2.45 (d, J = 4.0 Hz, 2H, CH$_2$), 1.87−1.86 (m, 1H, CH), 1.82 (d, J = 8.0 Hz, 3H, CH$_3$), 0.89 (d, J = 8.0 Hz, 6H, 2 × CH$_3$); ^{13}C NMR (100 MHz, CDCl$_3$) δ: 170.52, 160.29, 154.54, 148.83, 142.90, 141.24, 137.01, 133.73, 130.38, 129.69, 127.10, 126.70, 123.01, 119.75, 114.71, 45.02, 37.19, 30.17, 22.37, 19.66; HRMS (ESI) m/z: Anal. calcd for C$_{23}$H$_{21}$Cl$_2$N$_2$O$_3$ $[M + H]^+$: 443.0929, found: 443.0933 (M^+, 100); anal. RP-UPLC t_R = 29.108 min, purity 97.29%, UV 330 nm.

4.2.4.5. 6,8-Dibromo-3-(5-(1-(4-isobutylphenyl)ethyl)-1,3,4-oxadiazol-2-yl)-2H-chromen-2-one (8e). White solid. Mp: 226−228 °C; ^{1}H NMR (400 MHz, CDCl$_3$) δ: 8.42 (s, H, H-4 coumarin), 7.98−7.11 (m, 6H, ArH), 4.46 (q, J = 8.0 Hz, H, CH), 2.45 (d, J = 4.0 Hz, 2H, CH$_2$), 1.87−1.84 (m, 1H, CH), 1.82 (d, J = 8.0 Hz, 3H, CH$_3$), 0.89 (d, J = 8.0 Hz, 6H, 2 × CH$_3$); ^{13}C NMR (100 MHz, CDCl$_3$) δ: 170.49, 160.25, 154.83, 150.36, 142.81, 141.24, 139.27, 137.02, 130.44, 129.69, 127.11, 120.19, 117.68, 114.61, 111.54, 45.02, 37.19, 30.17, 22.38, 19.55; HRMS (ESI) m/z: Anal. calcd for C$_{23}$H$_{21}$Br$_2$N$_2$O$_3$ $[M + H]^+$: 530.9919, found: 530.9921 (M^+, 100); anal. RP-UPLC t_R = 29.544 min, purity 98.94%, UV 330 nm.

4.2.4.6. 3-(5-(1-(4-Isobutylphenyl)ethyl)-1,3,4-oxadiazol-2-yl)-6-methyl-2H-chromen-2-one (8f). White solid. Mp:136−137 °C; ^{1}H NMR (400 MHz, CDCl$_3$) δ: 8.47 (s, H, H-4 coumarin), 7.45−7.11 (m, 7H, ArH), 4.46 (q, J = 8.0 Hz, H, CH), 2.45−2.43 (m, 5H, 1 × CH$_2$ 1 × CH$_3$), 1.87−1.84 (m, 1H, CH), 1.82 (d, J = 4.0 Hz, 3H, CH$_3$), 0.89 (d, J = 8.0 Hz, 6H, 2 × CH$_3$); ^{13}C NMR (100 MHz, CDCl$_3$) δ: 170.01, 161.15, 156.58, 152.78, 144.89, 141.11, 137.27, 135.20, 135.04, 129.65, 128.82, 127.12, 117.78, 116.66, 112.65, 45.03, 37.17, 30.17, 22.39, 20.75, 19.74; HRMS (ESI) m/z: Anal. calcd for C$_{24}$H$_{25}$N$_2$O$_3$ $[M + H]^+$: 389.1865, found: 389.1867 (M^+, 100); anal. RP-UPLC t_R = 27.415 min, purity 99.83%, UV 330 nm.

4.3. Antitumor Activity Assay In Vitro. To evaluate the inhibiting effect of novel ibuprofen−coumarin hybrid compounds on HeLa cells and HEK293 cells, we performed the CCK8 assay.[54,55] First, the cells were seeded at a density of 5000 cells/well in a 96-well plate for culture and then incubated at 37 °C with 5% CO$_2$ for 24 h. Next, a serum-free medium containing different concentrations (1.0, 2.0, 4.0, 8.0, and 10.0 mg/L) of the compound was used. The non-medicated medium was a negative control, while an equal concentration of DMSO was a solvent control, and gefitinib

was a positive control. After 24 h of culture, the medium was discarded, cells were washed once with PBS, and then 10 μL of CCK8 enhanced solution medium was administered to each well. After 3 h of incubation, the supernatant was removed, and 150 μL of DMSO was added to each well. The absorbance of the 96-well plate was then measured at a wavelength of 490 nm, the cell inhibition rate = ((1 − A experiment)/A control) × 100%, and the IC$_{50}$ was calculated subsequently.

4.4. Kinase Assay. Seventy-five microliters of COX-2 assay buffer, 5 μL of COX-2 cofactor, 5 μL of rhCOX-2, and 5 μL of solvent (the same solvent used to dissolve the inhibitor) were added to 100% initial activity wells. Then, 80 μL of assay buffer, 5 μL of COX-2 cofactor, and 5 μL of solvent (the same solvent used to dissolve the inhibitor) were added to the background wells. Seventy-five microliters of COX-2 assay buffer, 5 μL of COX-2 cofactor, 5 μL of rhCOX-2, and 5 μL of inhibitor (10 μM, 2 μM, 400 nM, 80 nM, 16 nM, 3.2 nM, and 0.64 nM) were added to the inhibitor wells. Then, 5 μL of COX-2 Probe and 5 μL of COX-2 substrate were added to every well. The plate was incubated for 10 min at 37 °C. The plate was read using an excitation wavelength at 560 nm and an emission wavelength at 590 nm.

■ ASSOCIATED CONTENT

ⓢ Supporting Information

The Supporting Information is available free of charge at https://pubs.acs.org/doi/10.1021/acsomega.4c06596.

Computational experimental procedure; ^{1}H NMR, ^{13}C NMR spectra (Figures S4−S45), and HRMS (Figures S46−S66) of every synthesized compound have been listed (PDF)

■ AUTHOR INFORMATION

Corresponding Authors

Junkai Ma − *School of Pharmaceutical Sciences and Institute of Medicinal Chemistry, Hubei University of Medicine, Shiyan 442000, China; Hubei Key Laboratory of Wudang Local Chinese Medicine Research, Hubei University of Medicine, Shiyan 442000, China;* Email: majunkai17@hbmu.edu.cn

Yanggen Hu − *School of Pharmaceutical Sciences and Institute of Medicinal Chemistry, Hubei University of Medicine, Shiyan 442000, China; Hubei Key Laboratory of Wudang Local Chinese Medicine Research, Hubei University of Medicine, Shiyan 442000, China;* Email: huyg@hbmu.edu.cn

Authors

Fengxu Wu − *School of Pharmaceutical Sciences and Institute of Medicinal Chemistry, Hubei University of Medicine, Shiyan 442000, China; Hubei Key Laboratory of Wudang Local Chinese Medicine Research, Hubei University of Medicine, Shiyan 442000, China;* ⓞ orcid.org/0009-0004-8768-320X

Tianshuai Wang − *School of Pharmaceutical Sciences and Institute of Medicinal Chemistry, Hubei University of Medicine, Shiyan 442000, China; Hubei Key Laboratory of Wudang Local Chinese Medicine Research, Hubei University of Medicine, Shiyan 442000, China*

Xiaoyu Tang − *School of Pharmaceutical Sciences and Institute of Medicinal Chemistry, Hubei University of Medicine, Shiyan 442000, China; Hubei Key Laboratory of Wudang Local Chinese Medicine Research, Hubei University of Medicine, Shiyan 442000, China*

Sirui Dong − *Taihe Hospital, China Anti-aging Center of Affiliated Hospital of Hubei University of Medicine, Shiyan 442000, China*

Lun Luo − *School of Pharmaceutical Sciences and Institute of Medicinal Chemistry, Hubei University of Medicine, Shiyan 442000, China; Hubei Key Laboratory of Wudang Local Chinese Medicine Research, Hubei University of Medicine, Shiyan 442000, China*

Chao Luo − *Hubei Key Laboratory of Wudang Local Chinese Medicine Research and School of Basic Medical Sciences, Hubei University of Medicine, Shiyan 442000, China*

Complete contact information is available at:
https://pubs.acs.org/10.1021/acsomega.4c06596

Author Contributions

[⊥]F.W., T.W., and X.T. authors contributed equally to this work.

Notes

The authors declare no competing financial interest.

■ REFERENCES

(1) Sung, H.; Ferlay, J.; Siegel, R. L.; Laversanne, M.; Soerjomataram, I.; Jemal, A.; Bray, F. Global cancer statistics 2020: GLOBOCAN estimates of incidence and mortality worldwide for 36 cancers in 185 countries. *Ca-Cancer J. Clin.* **2021**, *71* (3), 209−249.

(2) Pin, F.; Couch, M. E.; Bonetto, A. Preservation of muscle mass as a strategy to reduce the toxic effects of cancer chemotherapy on body composition. *Curr. Opin. Supportive Palliative Care* **2018**, *12* (4), 420−426.

(3) Prieto-Callejero, B.; Rivera, F.; Fagundo-Rivera, J.; Romero, A.; Romero-Martín, M.; Gómez-Salgado, J.; Ruiz-Frutos, C. Relationship between chemotherapy-induced adverse reactions and health-related quality of life in patients with breast cancer. *Medicine* **2020**, *99* (33), No. e21695.

(4) Thomsen, M.; Vitetta, L. Adjunctive Treatments for the Prevention of Chemotherapy- and Radiotherapy-Induced Mucositis. *Integr. Cancer Ther.* **2018**, *17* (4), 1027−1047.

(5) Haldar, R.; Shaashua, L.; Lavon, H.; Lyons, Y. A.; Zmora, O.; Sharon, E.; Birnbaum, Y.; Allweis, T.; Sood, A. K.; Barshack, I.; Cole, S.; Ben-Eliyahu, S. Perioperative inhibition of β-adrenergic and COX2 signaling in a clinical trial in breast cancer patients improves tumor Ki-67 expression, serum cytokine levels, and PBMCs transcriptome. *Brain, Behav., Immun.* **2018**, *73*, 294−309.

(6) Singh, N.; Baby, D.; Rajguru, J. P.; Patil, P. B.; Thakkannavar, S. S.; Pujari, V. B. Inflammation and cancer. *Ann. Afr. Med.* **2019**, *18* (3), 121−126.

(7) Voronov, E.; Apte, R. N. Targeting the Tumor Microenvironment by Intervention in Interleukin-1 Biology. *Curr. Pharm. Des.* **2017**, *23* (32), 4893−4905.

(8) Yang, H.; Yang, X. F.; Wu, S. D.; Xiao, J. H. COX-2 in liver fibrosis. *Clin. Chim. Acta* **2020**, *506*, 196−203.

(9) Sharma, V.; Bhatia, P.; Alam, O.; Naim, M. J.; Nawaz, F.; Sheikh, A. A.; Jha, M. Recent advancement in the discovery and development of COX-2 inhibitors: Insight into biological activities and SAR studies (2008−2019). *Bioorg. Chem.* **2019**, *89*, 103007 DOI: 10.1016/j.bioorg.2019.103007.

(10) Tsuge, K.; Inazumi, T.; Shimamoto, A.; Sugimoto, Y. Molecular mechanisms underlying prostaglandin E$_2$-exacerbated inflammation and immune diseases. *Int. Immunol.* **2019**, *31* (9), 597−606.

(11) Haase-Kohn, C.; Laube, M.; Donat, C. K.; Belter, B.; Pietzsch, J. CRISPR/Cas9Mediated Knockout of Cyclooxygenase-2 Gene Inhibits Invasiveness in A2058 Melanoma Cells. *Cells* **2022**, *11* (4), 749.

(12) Lalrinzuali, K.; Vabeiryureilai, M.; Jagetia, G. C. Sonapatha (Oroxylum indicum) mediates cytotoxicity in cultured HeLa cells by inducing apoptosis and suppressing NF-KB, COX-2, RASSF7 and NRF2. *Bioorg. Chem.* **2021**, *114*, 105126 DOI: 10.1016/j.bioorg.2021.105126.

(13) Sun, G. S.; Sun, G. Q.; Chen, X.; Kong, X. Y.; Zheng, W. B.; Li, Z. T.; Zheng, Z. Y.; Cao, H. Y.; Lv, C. Y.; Xia, Y. X.; Tang, W. W. Meloxicam Inhibits Hepatocellular Carcinoma Progression and Enhances the Sensitivity of Immunotherapy via the MicroRNA-200/PD-L1 Pathway. *J. Oncol.* **2022**, *2022*, 4598573 DOI: 10.1155/2022/4598573.

(14) Basudhar, D.; Glynn, S. A.; Greer, M.; Somasundaram, V.; No, J. H.; Scheiblin, D. A.; Garrido, P.; Heinz, W. F.; Ryan, A. E.; Weiss, J. M.; Cheng, R. Y. S.; Ridnour, L. A.; Lockett, S. J.; McVicar, D. W.; Ambs, S.; Wink, D. A. Coexpression of NOS2 and COX2 accelerates tumor growth and reduces survival in estrogen receptor-negative breast cancer. *Proc. Natl. Acad. Sci. U.S.A.* **2017**, *114* (49), 13030−13035.

(15) Hashemi Goradel, N.; Najafi, M.; Salehi, E.; Farhood, B.; Mortezaee, K. Cyclooxygenase-2 in cancer: A review. *J. Cell Physiol.* **2019**, *234* (5), 5683−5699.

(16) Mizuno, R.; Kawada, K.; Sakai, Y. Prostaglandin E2/EP Signaling in the Tumor Microenvironment of Colorectal Cancer. *Int. J. Mol. Sci.* **2019**, *20* (24), 6254.

(17) Tołoczko-Iwaniuk, N.; Dziemianczyk-Pakiela, D.; Nowaszewska, B. K.; Celinska-Janowicz, K.; Miltyk, W. Celecoxib in Cancer Therapy and Prevention - Review. *Curr. Drug Targets* **2019**, *20* (3), 302−315.

(18) Irvine, J.; Afrose, A.; Islam, N. Formulation and delivery strategies of ibuprofen: challenges and opportunities. *Drug Dev. Ind. Pharm.* **2018**, *44* (2), 173−183.

(19) Shekelle, P. G.; Newberry, S. J.; FitzGerald, J. D.; Motala, A.; O'Hanlon, C. E.; Tariq, A.; Okunogbe, A.; Han, D.; Shanman, R. Management of Gout: A Systematic Review in Support of an American College of Physicians Clinical Practice Guideline. *Ann. Int. Med.* **2017**, *166* (1), 37−55.

(20) Kanabar, D. J. A clinical and safety review of paracetamol and ibuprofen in children. *Inflammopharmacology* **2017**, *25* (1), 1−9.

(21) Millecam, J.; van Bergen, T.; Schauvliege, S.; Antonissen, G.; Martens, A.; Chiers, K.; Gehring, R.; Gasthuys, E.; Vande Walley, J.; Croubels, S.; Devreese, M. Developmental Pharmacokinetics and Safety of Ibuprofen and Its Enantiomers in the Conventional Pig as Potential Pediatric Animal Model. *Front. Pharmacol.* **2019**, *10*, 505 DOI: 10.3389/fphar.2019.00505.

(22) Ziesenitz, V. C.; Zutter, A.; Erb, T.; van Den Anker, J. N. Efficacy and Safety of Ibuprofen in Infants Aged Between 3 and 6 Months. *Pediatr. Drugs* **2017**, *19* (4), 277−290.

(23) Shokri, B.; Zarghi, A.; Shahhoseini, S.; Mohammadi, R.; Kobarfard, F. Design, synthesis and biological evaluation of peptide-NSAID conjugates for targeted cancer therapy. *Arch. Pharm.* **2019**, *352* (8), 1800379 DOI: 10.1002/ardp.201800379.

(24) Özdemir, Ö.; Marinelli, L.; Cacciatore, I.; Ciulla, M.; Emsen, B.; Di Stefano, A.; Mardinoglu, A.; Turkez, H. Anticancer effects of novel NSAIDs derivatives on cultured human glioblastoma cells. *Z. Naturforsch. C* **2021**, *76* (7−8), 329−335.

(25) Albiero, L. R.; de Andrade, M. F.; Marchi, L. F.; Landi-Librandi, A. P.; de Figueiredo-Rinhel, A. S. G.; Carvalho, C. A.; Kabeya, L. M.; de Oliveira, R. D. R.; Azzolini, A.; Pupo, M. T.; Emery, F. D.; Lucisano-Valim, Y. M. Immunomodulating action of the 3-phenylcoumarin derivative 6,7-dihydroxy-3- 3′,4′-methylenedioxy-

phenyl -coumarin in neutrophils from patients with rheumatoid arthritis and in rats with acute joint inflammation. *Inflamm. Res.* **2020**, *69* (1), 115−130.

(26) Chandel, P.; Kumar, A.; Singla, N.; Kumar, A.; Singh, G.; Gill, R. K. Rationally synthesized coumarin based pyrazolines ameliorate carrageenan induced inflammation through COX-2/pro-inflammatory cytokine inhibition. *MedChemComm* **2019**, *10* (3), 421−430.

(27) Sen, Z.; Wang, W. D.; Ma, J.; Sheng, L.; Zhang, D. M.; Chen, X. G. Coumarin glycosides from *Hydrangea paniculata* slow down the progression of diabetic nephropathy by targeting Nrf2 anti-oxidation and smad2/3-mediated profibrosis. *Phytomedicine* **2019**, *57*, 385−395.

(28) Ying, T. H.; Lin, C. L.; Chen, P. N.; Wu, P. J.; Liu, C. J.; Hsieh, Y. H. Angelol-A exerts anti-metastatic and anti-angiogenic effects on human cervical carcinoma cells by modulating the phosphorylated-ERK/miR-29a-3p that targets the MMP2/VEGFA axis. *Life Sci.* **2022**, *296*, 120317.

(29) Eldehna, W. M.; Taghour, M. S.; Al-Warhi, T.; Nocentini, A.; Elbadawi, M. M.; Mahdy, H. A.; Abdelrahman, M. A.; Alotaibi, O. J.; Aljaeed, N.; Elimam, D. M.; Afarinkia, K.; Abdel-Aziz, H. A.; Supuran, C. T. Discovery of 2,4-thiazolidinedione-tethered coumarins as novel selective inhibitors for carbonic anhydrase IX and XII isoforms. *J. Enzyme Inhib. Med. Chem.* **2022**, *37* (1), 531−541.

(30) Batran, R. Z.; Dawood, D. H.; El-Seginy, S. A.; Ali, M. M.; Maher, T. J.; Gugnani, K. S.; Rondon-Ortiz, A. N. New Coumarin Derivatives as Anti-Breast and Anti-Cervical Cancer Agents Targeting VEGFR-2 and p38 MAPK. *Arch. Pharm.* **2017**, *350* (9), 1700064 DOI: 10.1002/ardp.201700064.

(31) Cacchio, A.; Prencipe, R.; Bertone, M.; De Benedictis, L.; Taglieri, L.; D'Elia, E.; Centoletti, C.; Di Carlo, G. Effectiveness and safety of a product containing diosmin, coumarin, and arbutin (Linfadren) in addition to complex decongestive therapy on management of breast cancer-related lymphedema. *Support. Care Cancer* **2019**, *27* (4), 1471−1480.

(32) Dhawan, S.; Kerru, N.; Awolade, P.; Singh-Pillay, A.; Saha, S. T.; Kaur, M.; Jonnalagadda, S. B. Shing, P. Synthesis, computational studies and antiproliferative activities of coumarin-tagged 1,3,4-oxadiazole conjugates against MDA-MB-231 and MCF-7 human breast cancer cells. *Bioorgan. Med. Chem.* **2018**, *26* (21), 5612−5623.

(33) Woodruff, S.; Lee, A. Y. Y.; Carrier, M.; Feugère, G.; Abreu, P.; Heissler, J. Low-molecular-weight-heparin versus a coumarin for the prevention of recurrent venous thromboembolism in high- and low-risk patients with active cancer: a post hoc analysis of the CLOT Study. *J. Thromb. Thrombolysis* **2019**, *47* (4), 495−504.

(34) Zhang, L.; Xu, Z. Coumarin-containing hybrids and their anticancer activities. *Eur. J. Med. Chem.* **2019**, *181*, 111587.

(35) Pilli, G.; Dumala, N.; Mattan, I.; Grover, P.; Prakash, M. J. Design, synthesis, biological and *in silico* evaluation of coumarin-hydrazone derivatives as tubulin targeted antiproliferative agents. *Bioorg. Chem.* **2019**, *91*, 103143 DOI: 10.1016/j.bioorg.2019.103143.

(36) Achar, G.; Shahini, C. R.; Patil, S. A.; Malecki, J. G.; Pan, S. H.; Lan, A.; Chen, X. R.; Budagumpi, S. Sterically modulated silver(I) complexes of coumarin substituted benzimidazol-2-ylidenes: Synthesis, crystal structures and evaluation of their antimicrobial and antilung cancer potentials. *J. Inorg. Biochem.* **2018**, *183*, 43−57.

(37) Channar, P. A.; Irum, H.; Mahmood, A.; Shabir, G.; Zaib, S.; Saeed, A.; Ashraf, Z.; Larik, F. A.; Lecka, J.; Sévigny, J.; Iqbal, J. Design, synthesis and biological evaluation of trinary benzocoumarin-thiazoles-azomethines derivatives as effective and selective inhibitors of alkaline phosphatase. *Bioorg. Chem.* **2019**, *91*, 103137.

(38) Mei, L.; Wu, F.; Hao, G.; Yang, G. Protocol for hit-to-lead optimization of compounds by auto in silico ligand directing evolution (AILDE) approach. *STAR Protoc.* **2021**, *2* (1), No. 100312.

(39) Shi, J.; Cao, H.; Wang, C.; Gao, S.; Wang, J.; Zhao, L.; Ye, F.; Fu, Y. In silico approach of novel HPPD/PDS dual target inhibitors by pharmacophore, AILDE and molecular docking. *J. Taiwan Inst. Chem. Eng.* **2023**, *143*, 104711.

(40) Shi, J.; Gao, S.; Wang, J.; Ye, T.; Yue, M.; Fu, Y.; Ye, F. Computer-Aided and AILDE Approaches to Design Novel 4-Hydroxyphenylpyruvate Dioxygenase Inhibitors. *Int. J. Mol. Sci.* **2022**, *23* (14), 7822.

(41) Wu, F.; Zhuo, L.; Wang, F.; Huang, W.; Hao, G.; Yang, G. Auto *In Silico* Ligand Directing Evolution to Facilitate the Rapid and Efficient Discovery of Drug Lead. *Iscience* **2020**, *23* (6), 101179 DOI: 10.1016/j.isci.2020.101179.

(42) Kulkarni, S.; Rader, J. S.; Zhang, F.; Liapis, H.; Koki, A. T.; Masferrer, J. L.; Subbaramaiah, K.; Dannenberg, A. J. Cyclooxygenase-2 is overexpressed in human cervical cancer. *Clin. Cancer Res.* **2001**, *7* (2), 429−434.

(43) Li, Y.; Pu, D.; Li, Y. The expression of cyclooxygenase-2 in cervical cancers and Hela cells was regulated by estrogen/progestogen. *J. Huazhong Univ. Sci. Technol.* **2007**, *27* (4), 457−460.

(44) Mao, Y.; Wang, L.; Xu, C.; Han, S. Effect of photodynamic therapy combined with Celecoxib on expression of cyclooxygenase-2 protein in HeLa cells. *Oncol. Lett.* **2018**, *15* (5), 6599−6603.

(45) Wang, A. H.; Tian, X. Y.; Yu, J. J.; Mi, J. Q.; Liu, H.; Wang, R. F. Celecoxib Radiosensitizes the Human Cervical Cancer HeLa Cell Line via a Mechanism Dependent on Reduced cyclo-oxygenase-2 and Vascular Endothelial Growth Factor C Expression. *J. Int. Med. Res.* **2012**, *40* (1), 56−66.

(46) Hou, T.; Wang, J.; Li, Y.; Wang, W. Assessing the Performance of the MM/PBSA and MM/GBSA Methods. 1. The Accuracy of Binding Free Energy Calculations Based on Molecular Dynamics Simulations. *J. Chem. Inf. Model.* **2011**, *51* (1), 69−82.

(47) Miciaccia, M.; Belviso, B. D.; Iaselli, M.; Cingolani, G.; Ferorelli, S.; Cappellari, M.; Loguercio Polosa, P.; Perrone, M. G.; Caliandro, R.; Scilimati, A. Three-dimensional structure of human cyclooxygenase (hCOX)-1. *Sci. Rep.* **2021**, *11* (1), No. 4312.

(48) Lucido, M. J.; Orlando, B. J.; Vecchio, A. J.; Malkowski, M. G. Crystal Structure of Aspirin-Acetylated Human Cyclooxygenase-2: Insight into the Formation of Products with Reversed Stereochemistry. *Biochemistry* **2016**, *55* (8), 1226−1238.

(49) Rose, P. W.; Prlic, A.; Altunkaya, A.; Bi, C.; Bradley, A. R.; Christie, C. H.; Di Costanzo, L.; Duarte, J. M.; Dutta, S.; Feng, Z.; Green, R. K.; Goodsell, D. S.; Hudson, B.; Kalro, T.; Lowe, R.; Peisach, E.; Randle, C.; Rose, A. S.; Shao, C.; Tao, Y.-P.; Valasatava, Y.; Voigt, M.; Westbrook, J. D.; Woo, J.; Yang, H.; Young, J. Y.; Zardecki, C.; Berman, H. M.; Burley, S. K. The RCSB protein data bank: integrative view of protein, gene and 3D structural information. *Nucleic. Acids. Res.* **2017**, *45* (D1), gkw1000.

(50) Durrant, J. D.; Amaro, R. E.; McCammon, J. A. AutoGrow: a novel algorithm for protein inhibitor design. *Chem. Biol. Drug Des.* **2009**, *73* (2), 168−178.

(51) Ho, W.; Kukla, M. J.; Breslin, H. J.; Ludovici, D. W.; Grous, P. P.; Diamond, C. J.; Miranda, M.; Rodgers, J. D.; Ho, C. Y.; Declercq, E.; Pauwels, R.; Andries, K.; Janssen, M. A. C.; Janssen, P. A. J. Synthesis and anti-HIV-1 activity of 4,5,6,7-tetrahydro-5-methylimidazo 4,5,1-jk 1,4 benzodazepin-2(1*H*)-one (TIBO) derivatives. 4. *J. Med. Chem.* **1995**, *38* (5), 794−802.

(52) Smith, R. H., Jr.; Jorgensen, W. L.; Tirado-Rives, J.; Lamb, M. L.; Janssen, P. A.; Michejda, C. J.; Kroeger Smith, M. B. Prediction of binding affinities for TIBO inhibitors of HIV-1 reverse transcriptase using Monte Carlo simulations in a linear response method. *J. Med. Chem.* **1998**, *41* (26), 5272−5286.

(53) Wang, J.; Morin, P.; Wang, W.; Kollman, P. A. Use of MM-PBSA in reproducing the binding free energies to HIV-1 RT of TIBO derivatives and predicting the binding mode to HIV-1 RT of efavirenz by docking and MM-PBSA. *J. Am. Chem. Soc.* **2001**, *123* (22), 5221−5230.

(54) Hu, Y. G.; Wang, Y.; Du, S. M.; Chen, X. B.; Ding, M. W. Efficient synthesis and biological evaluation of some 2,4-diamino-furo 2,3-*d* pyrimidine derivatives. *Bioorg. Med. Chem. Lett.* **2010**, *20* (21), 6188−6190.

(55) Jin, Y.; He, S. J.; Wu, F. X.; Luo, C.; Ma, J. K.; Hu, Y. G. Novel Coumarin-furo 2,3-d pyrimidinone hybrid derivatives as anticancer agents: Synthesis, biological evaluation and molecular docking. *Eur. J. Pharm. Sci.* **2023**, *188*, 106520.